AERODYNAMIC TESTS OF THE FUSELAGE OF ITA'S UNMANNED AERIAL VEHICLE

Roberto da Mota Girardi
Instituto Tecnológico de Aeronáutica (ITA). Praça Mal. Eduardo Gomes, 50, S J Campos – SP, Brasil
girardi@ita.br

André Valdetaro Gomes Cavalieri
Instituto Tecnológico de Aeronáutica (ITA). Praça Mal. Eduardo Gomes, 50, S J Campos – SP, Brasil
andre@ita.br

Tiago Barbosa de Araújo
Instituto Tecnológico de Aeronáutica (ITA). Praça Mal. Eduardo Gomes, 50, S J Campos – SP, Brasil
araujotb@ita.br

Abstract. *Unmanned Aerial Vehicles (UAV) have became more important in the last years, due to the low prices of electronic systems required for the guidance and control of an aircraft. This kind of vehicle is capable of performing a large number of missions with lower costs compared to manned aircraft. The UAV studied in this work must inspect the elements of an energy transmission line, that is, the towers, the cables and the nearby vegetation. The speed of the aircraft should be relatively low (close to 80 km/h) and, thus, it is necessary to obtain an aerodynamics database for low Reynolds numbers. This work presents the experimental work performed in order to obtain the fuselage aerodynamic coefficients (CL, CM and CD) of the ITA's UAV for a range of angles of attack, at the cruise Reynolds number. The flow over the fuselage is also studied with visualizations, which allow the detection of boundary layer separation at the surface. The results lead to an approach for fuselage project more appropriate for the range of Reynolds numbers typical of unmanned aerial vehicles.*

Keywords*: Unmanned Aircraft Vehicle, fuselage, Experimental and Numerical Methods, Aerodynamic center determination*

1. INTRODUCTION

Unmanned aircraft vehicles (UAV) can be used in several civil applications, like that: (i) Electrical lines and pipelines examination, (ii) harbors, forest reservations and less accessible frontiers vigilance, (iii) aircraft and disappeared people rescue, (iv) aerial picture generation and (v) others.

In 2004 Technological Institute of Aeronautics (ITA) was contacted to participate in a cooperation involving Advanced System Studies Center of Recife (CESAR) and São Francisco Electric Company (CHESF). The goal of such cooperation was an UAV development, for electrical line elements (towers, vegetation existing in the neighborhood of electrical lines, electrical connectors at the towers and etc) examination. In order to accomplish this task, a very low velocity (80 km/h) aircraft, flying at low altitude, is required, due to infrared camera limitations (required to observe hot spots, which indicate electric problems at some line elements). In such velocity range, atmospheric gusts became very important due to these effects on the flight security and because the electric line elements examination mission became very difficult, due the constant aircraft attitude changes.

The low aircraft velocity, required to accomplish the infrared camera examination mission, is in the inferior limit of an airplane flight envelope, because a high wing loading (W/S) is necessary to give the aircraft a low sensibility to atmospheric gusts, but, on the other hand, a low value of W/S is required to accomplish the low velocity flight requirement. All mission requirements could be fulfilled by using other kinds of aircrafts, like a helicopter, a dirigible or a hybrid vehicle, that is, a mixture between a dirigible and an airplane, for example. The most adapted kind of aircraft was analyzed by Girardi and Rizzi (2005a), where an airplane was chosen to be the kind of aircraft used in this project.

The second step in the conceptual phase of the airplane project was the definition of the more adapted configuration, considering all requirements fulfillment. Two basic airplane configurations were considered: (i) in the first one the engine is located at the airplane nose, a conventional tail was chosen to give stability and control to the aircraft and the camera was located at the fuselage low surface, near the aircraft gravity center (GC). (ii) In the second configuration, the engine was located at the fuselage tail, in the pusher configuration, and two booms were used to assembly the tail to the wing. In this configuration, the camera could be located at the fuselage nose or in the same place of the first configuration. Both configurations have high wing position (relative to the fuselage), a tricycle landing gear type and a rectangular wing. These configurations were analyzed by Girardi and Rizzi, (2005b) and the first one was chosen, considering the camera position near the aircraft GC (better to decrease effects on the camera due to the aircraft constant attitude changes, associated to the gusts effects) and the design team experience.

The aircraft conceptual design phase was executed by the Aeronautics Department of ITA and a special methodology was developed (Girardi e Rizzi, 2006) to face the problems associated to the airplane specific mission,

that is, image acquisition from an aircraft at low velocity, manufactured with non conventional material and subjected to atmospheric gusts, because of the low altitude required by the infrared imaging. In such methodology, the aircraft dimensions were determined considering the autopilot characteristics and this is an important aspect of the adopted procedure to this UAV design.

The work reported in this paper is inserted into the preliminary design phase, where more accurate information has to be used in order to improve the analysis methods used to determine the airplane dimensions, as well as, the relative positions of the different aircraft parts (wing, fuselage and tail). One of the problems verified during the conceptual design phase was the lack of information on low Reynolds number aerodynamic data, required to a small vehicle at low velocity. Such kind of information is very useful to generate the aircraft characteristic curves (CL x α, CL x Cm and the drag polar), which are used to performance, as well as, stability and control calculations.

During the aircraft design conceptual phase, the aerodynamic characteristics of the fuselage are generated by using a semi-empirical methodology (Roskam, 2000-2003 and Raymer, 1999), where fuselage is considered a body of revolution. The friction drag is estimated by using the flat plate friction coefficient and the fuselage wetted area and the pressure drag is estimated by using a simple function of the relation between the fuselage length (l_f) and maximum diameter (d_f). It is important to note that such function was obtained to full scale airplanes, where Reynolds number is high. For low Reynolds number cases, the above formula can furnish wrong information on the drag coefficient for angle of attack (α) equal to zero. When α is varied, the semi-empirical methodology is based on the circular cylinder drag coefficient and on the wind velocity component normal to the fuselage axis. This normal force is then decomposed in the undisturbed flow direction to obtain the fuselage induced drag.

The actual UAV fuselage is not a body of revolution. It has a rectangular cross section and, along its length, it is constituted by: (i) a small nose, containing the engine and its support, (ii) a constant cross section area part, where fuel tank, parachute, cameras, electronic equipment for guidance and control and batteries are installed and, finally, (iii) a trailing cone, characterized by a cross section area reduction, performed with the lower surface inclination. The upper trailing cone surface is in the same plane of the constant cross section area part of the fuselage. In this case, the flow field along the fuselage lower surface changes direction at the interface between trailing cone and fuselage central part and, depending on the inclination angle, flow separation can occurs, resulting in drag increment. Due to longitudinal vortex, generated at the corner formed by the intersection of lateral and lower surfaces of the trailing cone, induced drag occurs and it is incremented with the trailing cone inclination angle.

The objective of this paper is to present experimental results to the aerodynamic characteristic curves of the UAV fuselage, at low Reynolds number. The experiments were performed in an open circuit wind tunnel and a three component balance was used to obtain lift, drag and pitch moment of a half fuselage model (balance is assembled at the wind tunnel lateral wall). Wool tufts were used to allow flow visualization of the model at several angles of attack, in order to generate information to perform experimental result analysis. Two fuselage models were tested and the only difference between them is the corners shape: (i) in the first model, sharp corners are considered and (ii) in the second one, all model corners are rounded.

Finally, the experimental results are compared with the semi-empirical methodology mentioned above to verify its applicability to the specific fuselage used for the UAV developed at ITA. This comparison allows improvement of the semi-empirical method and, therefore, more reliable aerodynamic characteristic curves could be generated to future fuselage, with similar shape and subjected to a flow with similar Reynolds number.

2 EXPERIMENTAL APPARATUS

The measurements were performed in a blower wind tunnel with square test section, characterized by a dimension of 460 mm. The flow velocity ranges from 4 to 30 m/s and the turbulence intensity is 0.5% at the maximum velocity. Along the test section length the cross section area is changed in order to compensate the boundary-layer growth and, as a consequence, to keep a constant static pressure. This area change is performed by filling the test section corners with triangular elements, whose dimension changes along test section length, as shown in the Fig. 3(b).

Lift, drag and pitch moment of a model are measured with a balance fixed at the test section lateral wall (outside the wind tunnel). Aerodynamic forces and moment on the model are transmitted to the balance through a metal axis. Such balance has a triangular plate used to fix the metal axis originated at the model. The triangular plate is connected to the wind tunnel structure by using three load cells (metal plates, instrumented with four strain gages each, in order to assembly a complete Wheatstone bridge). Two of these load cells are used to make measurement of lift and pitch moment (sensors A and F) and the third one is used to obtain drag force measurements (sensor D). Each load cell is connected to an independent signal conditioner module (amplifier and filter), which allows adjustment of the output voltage considering the data acquisition board characteristics. For the present experiment, the maximum output voltage of each sensor is chosen to be 10 volts, which maximize measurements resolution.

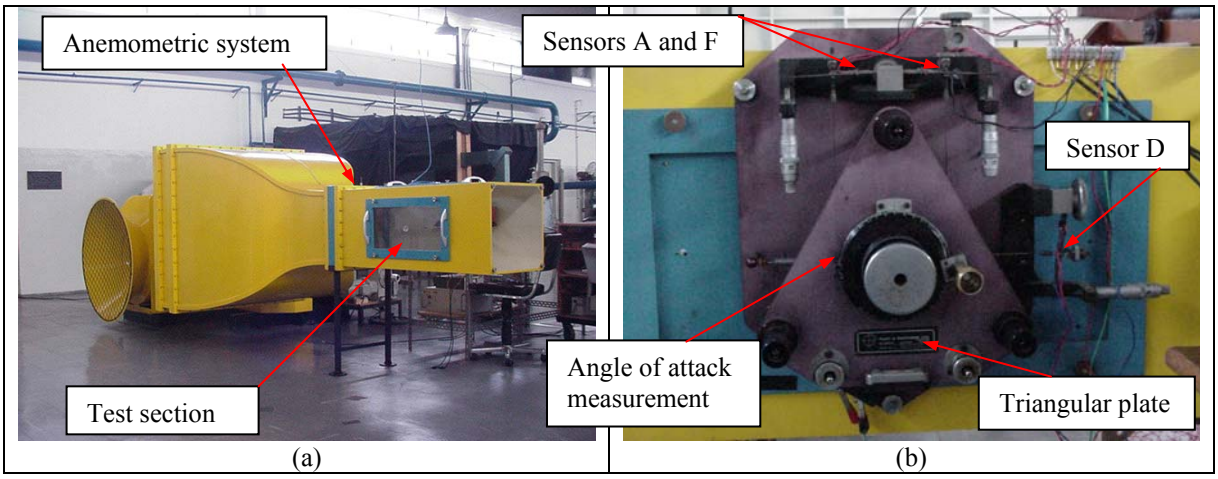

Figure 1: (a) Open circuit wind tunnel and (b) three component aerodynamic balance.

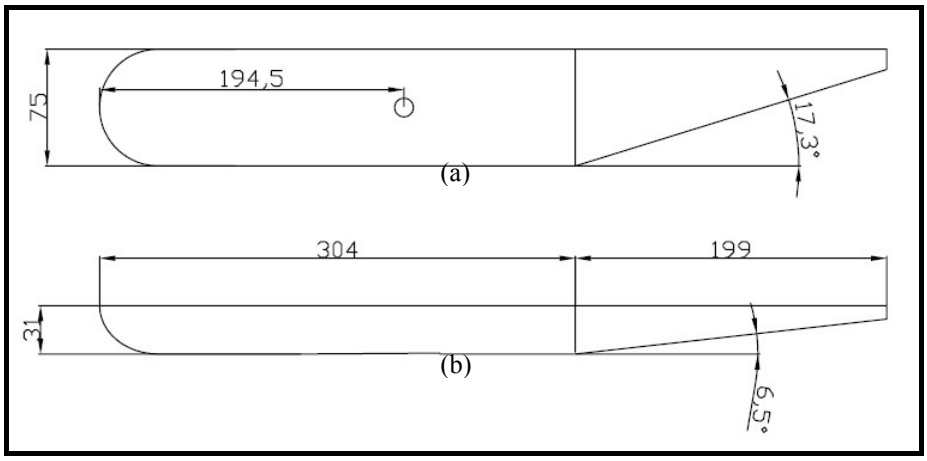

Figure 2: Fuselage half model: (a) Lateral view and (b) plan view . Dimensions in mm.

The dynamic and static pressures are measured by using a Pitot tube located at the beginning of the test section (tunnel anemometric system), just after the end of the contraction section, as can be seen in the figure 1(a). Pressure transducers are connected to the Pitot tube and a signal conditioner is used to amplify the output voltages before the connection with the data acquisition board.

The model angle of attack is varied manually and its measurement is performed by a rotating device (where the model axis is fixed) divided in 360 equal parts. The uncertainty of ± 0.5 degrees can be considered to this measurement.

Due to the balance configuration, the aerodynamic tests have to be performed with a fuselage half model, as shown in the figure 2. The fuselage model was manufactured with wood and it has the following characteristics: (i) a small nose region, designed to avoid flow separation of the oncoming flow and, therefore, minimize disturbances on the flow over the downstream fuselage region, (ii) a constant rectangular cross section part, with 75 mm high and 31 mm width and, (iii) a trailing cone, where the cross section area decreases along the model longitudinal axis. Such area variation is obtained through inclination of both lateral surfaces (6,5^{o} each one) and the lower one (17,3^{o}), as can be seen in the Fig. 2. The trailing cone upper surface is kept aligned to the fuselage central part and this surface is used as the model reference axis. The model is 503 mm total length and a steel axis is fixed at 194,5 mm from the model nose (see Fig. 3a) and it is used to fix the model to the aerodynamic balance. The model frontal area (used as the reference area for the aerodynamic coefficients) is 0.0023 m^2. Considering the test section cross section area, the model blockage ratio is approximately 1,1% and, therefore, the test section walls interference on the model flow is very low.

For half model testes, the model symmetrical plane (wind tunnel wall) should be a flow stream plane and the wall boundary layer flow should be eliminated to accomplish rigorously such requirement. One end plate (see Fig. 3b) is used to isolate the wind tunnel boundary layer from the flow over the fuselage model, in order to approximate the flow over the model to the free flight flow. The experimental results reported by Kubo (1989), were used, initially, to define the end plates dimensions. The distance the end plates are fixed from the wind tunnel lateral walls are defined as a function of the boundary layer thickness, determined in a previous work by using a hot wire anemometer.

After experiments conducted with an airfoil model, a flow field between the two sides of the end plates was observed, generating longitudinal vortices along the upper and lower edges of the end plate and causing great

disturbances on the model flow. Such problem is discussed in Girardi et alli (2007) and the problem was solved with an end plate spanning the test section high (see Fig. 3b), to avoid flow communication through the upper and lower edges of the end plate. The same end plate configuration was used in the present work.

Figure 3: (a) Half fuselage model and its metal axis and (b) rear view of the model inside the wind tunnel test section.

3. EXPERIMENTAL PROCEDURE

In the present work, the following measurements have to be performed: (i) the forces and pitch moment of the complete model configuration, (ii) the dynamic pressure, necessary to obtain the non-dimensional coefficients for lift (Cl), drag (Cd) and pitch moment (Cm). In this paper section, the experimental procedure established to determine each one of the above parameters is described, in order to show all care taken to guarantee reliable results.

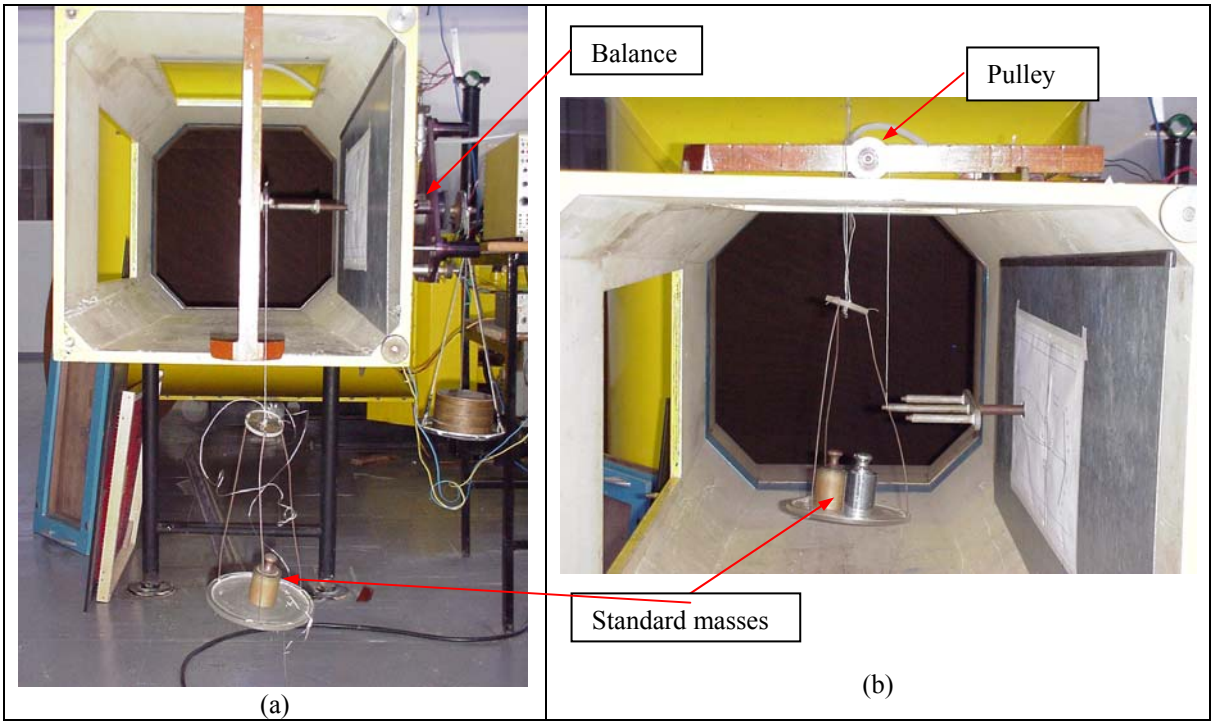

Figure 4: Aerodynamic balance calibration apparatus: (a) drag sensor and (b) Two other sensors used to obtain lift and pitch moment.

As mentioned in the preceding section, lift, drag and pitch moment are measured by using an aerodynamic balance, with three load cells. The first task to be done is the load cells calibration, in order to obtain a correlation between the force acting on each load cell with the voltage read by the acquisition system. The calibration procedure is

performed by incrementing loads from zero to the maximum value estimated for the specific sensor of the balance and, after that, a decrement is done up to zero again. At least 20 measures are used for the calibration process, in order to determine statistic parameters, used to uncertainties estimates. During such procedure, a small amount of vibration is used to decrease the time required to the balance structural parts accommodation and it is worth to note that such vibration is kept during the sampling process, performed by the data acquisition system. In the calibration procedure, one thousand measures were performed during a sampling time of one second and just a value (average of 1000) of voltage is correlated to the force imposed on the load cell. Each balance sensor is loaded by using calibrated masses and a system constituted by cables and pulleys, responsible to apply the force to an axis connected to the balance, as can be seen in the figure X. The three balance sensors are calibrated in two steps: (i) the load cell associated to the drag force is calibrated alone but (ii) for the other two sensors, the vertical load applied to the axis connected to the balance is divided by two and the load cells associated to the lift and pitch moment are calibrated simultaneously.

At the region where anemometric system is located (at the beginning of the test section) the flow field is distorted, due to the area variation along the contraction, causing errors in the values measured for the dynamic and static pressures. This problem can be corrected by performing a calibration procedure, where a Pitot tube, placed at the test section central region (location where models are tested) is compared with the anemometric system fixed at the wind tunnel. Calibration curves for the dynamic and static pressures are the results of the above procedure and they are used to correct the experimental results obtained with the wind tunnel anemometric system (The Pitot tube at the test section central region is withdrawn during the model experiments). The above calibration curves are incorporated in a computer code used to make calculations of the aerodynamic coefficients.

As mentioned in the previous section, the dynamic pressure is measured by using a pressure transducer, ranging from zero to 100 mm of water. A Betz manometer, with least count of 0,1 mm of water, is used as standard for the pressure transducer calibration, which is performed in the following way: (i) Initially, the pressure is increased and decreased several times (minimum of three) in order to get a repeatable measure of zero gage pressure at the Betz manometer. With such procedure, the internal walls of the Betz manometer are wetted. (ii) Starting from zero, the pressure is increased up to 50 mm of water, in steps of 5 mm and then (iii) pressure is decreased, using the same steps, up to zero again. For each point of the calibration curve, one thousand measures are collected during one second after the pressure stabilization (observed at the Betz manometer). The data acquisition code, written in LabView ambient, presents the linear fit of the experimental data and the standard deviations associated with the uncontrolled parameters of the experimental setup (random errors). These parameters are used to estimate the uncertainties associated to the aerodynamic coefficients.

After the calibration phase was finished, the experiment can be run in the following manner: (i) the end plate is assembled inside the wind tunnel test section, whose longitudinal axis is stamped on the end plate surface in order to allow model alignment. (ii) The fuselage model is fixed to the wind tunnel aerodynamic balance (through its metal axis) and initial alignment is performed, comparing the fuselage model upper surface with the longitudinal axis stamped on the end plate surface. (iii) Before starting the wind tunnel, all sensor signals are read by the data acquisition system (initial voltages). This operation is performed after some vibration was introduced, in a similar manner used during the aerodynamic balance calibration (see preceding section), in order to guarantee all load cells are well accommodated to the loads associated the zero dynamic pressure. The initial voltage accuracies are very important because all force measurements accuracies depend on them. It is worth to note that the aerodynamic forces and moments are obtained through the difference between the sensor signal (voltage), measured with wind tunnel turned on, and the initial voltage (obtained with flow velocity equal to zero). (iv) In the next step, wind tunnel is turned on and the dynamic pressure required to the specific test is established. (v) The following results are typically obtained in an aerodynamic test program: The drag polar (Cd x CL), Cl x α and Cm x α. With the dynamic pressure fixed at a required value (associated to the Reynolds number) the angle of attack (α) is varied. In general, such variation starts at a negative angle of attack and increments of 1 degree are used. (vi) During the experiments described above, a data acquisition code, written in the LabView ambient, is used to make the measurements of the aerodynamic balance sensors (three) and the pressure transducer, used to register the wind tunnel dynamic pressure. For each angle of attack, whose value is inserted through the keyboard, the four sensor signals, are sampled 2000 times, using sampling rate of 200 hz. The resulting sample time of 10 seconds was chosen to account for the wind tunnel dynamic pressure variations and an average value is obtained for each parameter measured in this experiment. (vii) Data reduction is performed with other computational code, written in the LabView ambient, where the data generated to each sensor (voltages) is combined with the calibration curves to determine forces and moments acting on the model. Ambient pressure and temperature are used to calculate air density and dynamic viscosity. These parameters are combined with the dynamic pressure to calculate the test Reynolds number. Finally, the model reference area (model frontal area) and dimension (model high) together with the forces and moments are used to determine the aerodynamic coefficients mentioned previously.

Data generated during calibration procedure, as well as, during the experiment are used to determine the uncertainty associated to each aerodynamic coefficient. The uncertainty analysis was made by using the procedure described by Kline and Mcintoch (1953).

4. ANALYSIS OF RESULTS

The first task in this paper section is a description of the flow field around the fuselage model, based on the flow visualizations performed with wool tufts, as can be seen in the Figs 5 and 6. When the model angle of attack is different from zero, it is observed the presence of longitudinal vortices, originated at the model longitudinal edges. A very low pressure region is established along a vortex core and any surface near such vortex core is contaminated with the core region pressure. Increments of vortex strength (its circulation) are associated with lower values for the core region pressure and with induced drag increments.

When the angle of attack is negative, as shown in the Fig 5(a), two longitudinal vortices are generated at the model longitudinal corners. Vortex B, formed along the model upper corner, is established near the lateral surface and do not have direct influence on the lift force or on the pitch moment acting on the fuselage model. Vortex A, originated at the lower corner, is positioned near the model lower surface, which is contaminated with the low pressure of the vortex core region. Due to this fact, the fuselage lift force is incremented, as occurs in a delta wing case. Once the vortex strength is increased with the angle of attack, the lift force is incremented in a non-linear way, as can be seen in the Fig. 7, for negative angles of attack. A similar pattern is observed for positive angle of attacks, but, in this situation, vortex A, established near the model lateral surface, do no have direct influence on the lift force and on the pitch moment. On the other hand, vortex B, originated at the upper corner, is correlated to the pressure decrement on the model upper surface and it is associated with the non-linear lift curve behavior, as can be seen in the Fig.7, for positive angles of attack.

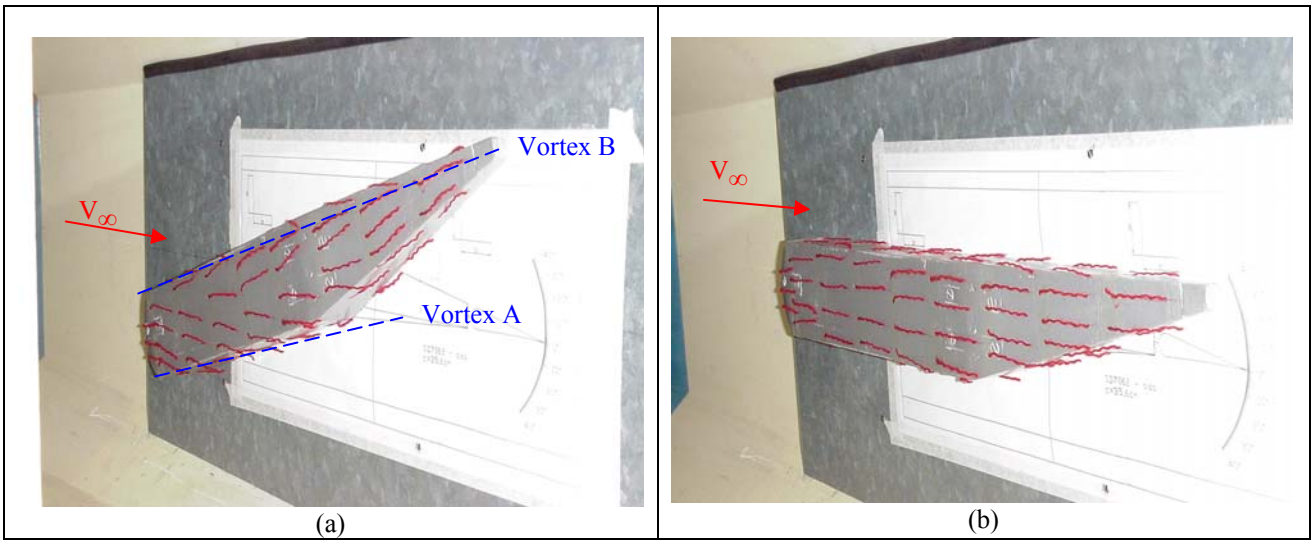

Figure 5: Flow visualization for the fuselage model: (a) Angle of attack (α) = -20^o and (b) (α) = 0^o.

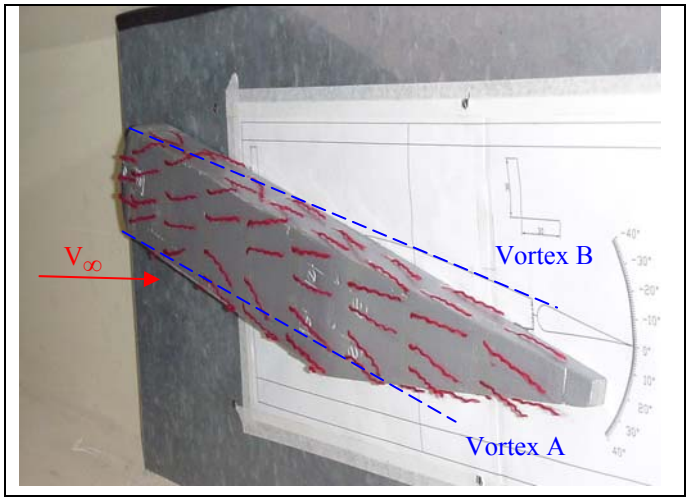

Figure 6: Flow visualization for the fuselage model for angle of attack (α) = +20^o.

A difference between the experimental results can be observed, in the Fig. 7, for the sharp and rounded models. Such difference is associated with the strength of the vortex formed along the model longitudinal corners. A greater strength is observed for the sharp corner model and, therefore, the lift force module is greater for positive and negative angles of attack. The above analysis can explain the lift curves crossing, observed in the Fig. 7.

Due to the fuselage shape and model dimensions, the lift and the pitch moment magnitudes are very low when compared with the models usually tested in the wind tunnel used in this research and, therefore, the load cells used to make measurements of these parameters are stiffer than it should be. Some erratic variations observed in the Fig. 7 are a consequence of the above explanation and could be improved with more flexible load cells. Unfortunately these equipments were not available during the experiments but, more adequate load cells will be developed to improve the experimental results quality in future works.

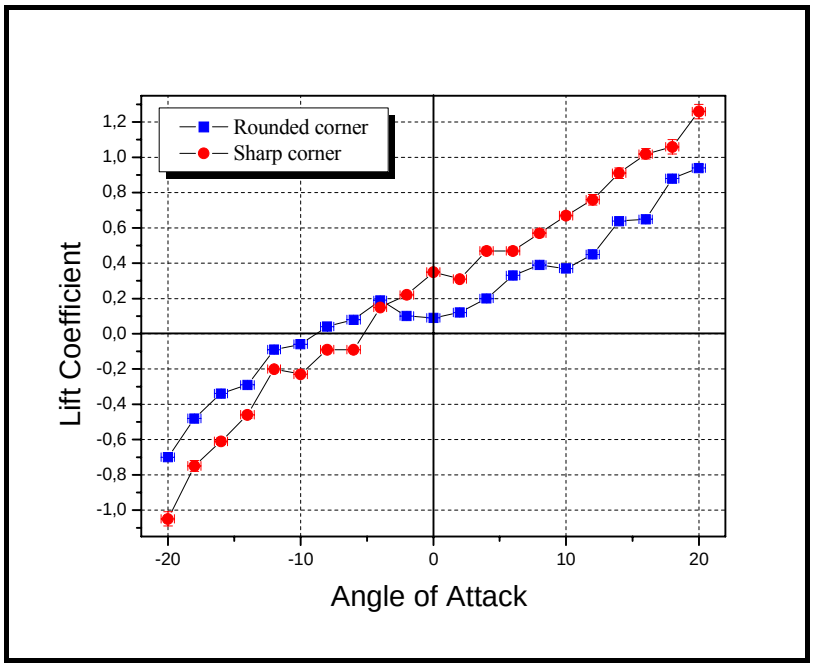

Figure 7: Lift coefficient as a function of the angle of attack, for the fuselage models

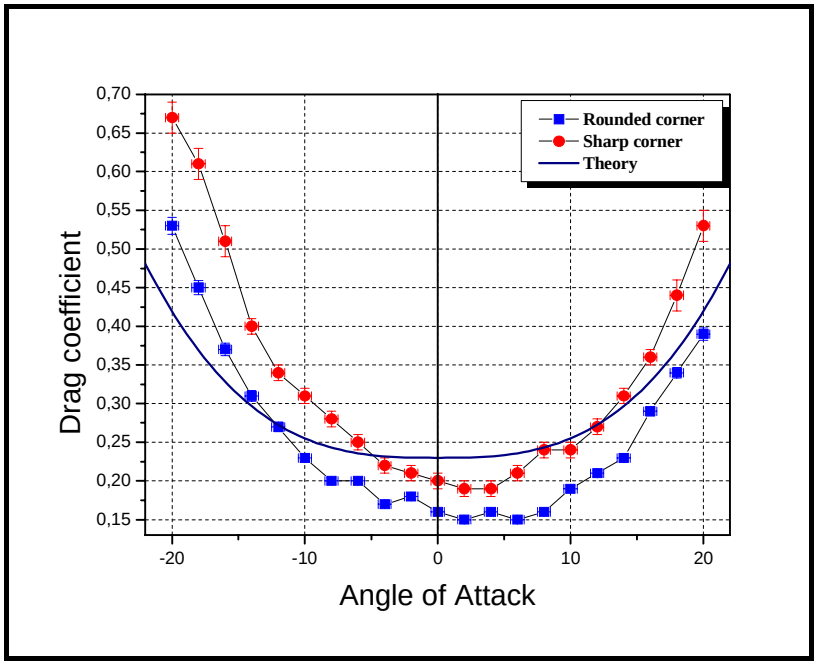

Figure 8: Drag coefficient as a function of the angle of attack, for the fuselage models

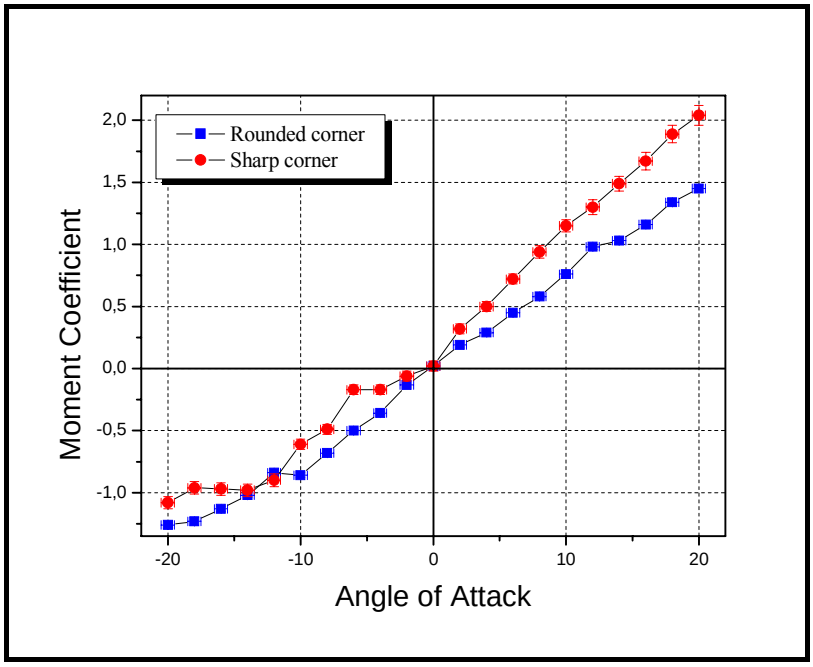

Figure 9: Pitch moment coefficient as a function of the angle of attack, for the fuselage models

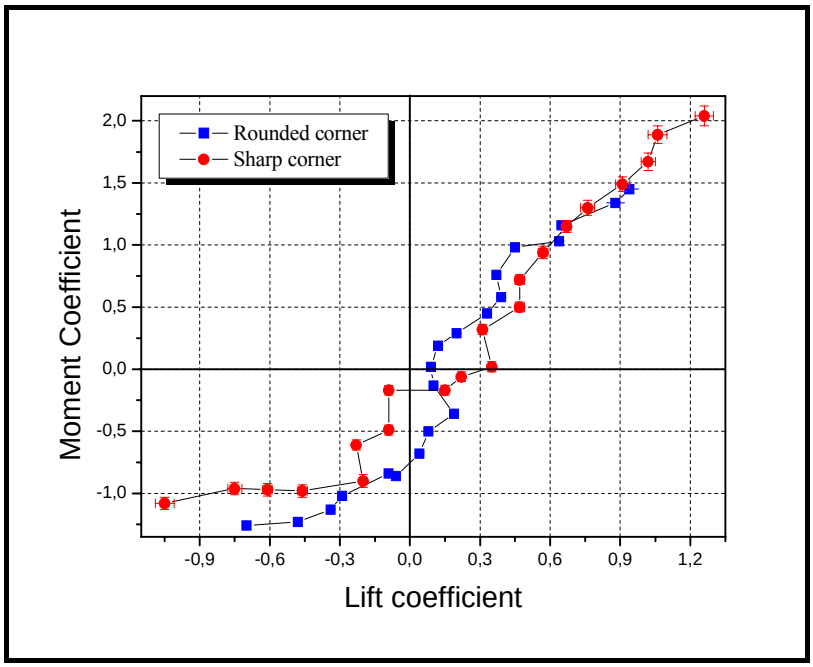

Figure 10: Pitch moment coefficient as a function of the lift coefficient, for the fuselage models

As expected, the rounded corner fuselage has lower value for the drag coefficient (Cd), as can be observed in the Fig. 8, even when the angle of attack is zero, that is, the fuselage longitudinal edges are aligned with the undisturbed flow. The cause for the Cd difference, for α=0, are the edges formed by the intersection between the lower and the lateral surfaces of the trailing cone. Due to the flow direction difference over each surface, longitudinal vortices are formed along these edges and cause induced drag. As mentioned before, the vortex strength is greater for the sharp corner configuration and this can explain the greater values for the Cd of such configuration. It is important to note that an attached flow was observed (using flow visualization) over the trailing cone lower surface. This flow characteristic is very important to avoid a large wake formation, which is associated to greater values for the drag coefficient (pressure drag). On the other hand, the same characteristic is responsible for a larger induced drag (correlated with the longitudinal vortices) as mentioned before.

As mentioned before, due to angle of attack increments the longitudinal vortices strength and the induced drag are increased and this is the explanation for the drag coefficient curve shape. The difference between the sharp and

rounded corner fuselage drag increases slightly with the angle of attack. Such behavior is correlated to the fact the sharp corner fuselage generates more strength vortex. The semi-empirical model (see Roskam, 2000-2003), discussed at the introduction of the present paper, was applied to the fuselage tested and its result is plotted in the Fig. 8. The drag coefficient, for lift equal to zero (Cd_0), is over estimated in approximately 40%. The drag coefficient variation with the angle of attack (induced drag) is under estimated by the semi-empirical method, probably because the longitudinal vortices are not considered and they are correlated to the induced drag.

The pitch moment coefficient (Cm), related to the model metal axis, as a function of the angle of attack is shown in the Fig. 9. Again, an erratic behavior is observed and this is associated to the problem, mentioned before, of the load cells stiffness used to make measurements of the lift force and the pitch moment. With the angle of attack the pitch moment is increased and this is a consequence of the force generated at the fuselage nose region, due to the flow acceleration around the nose. For positive angle of attacks, upward forces are generated at the nose region and cause positive pitch moment (that is, nose up moment). A slightly non-linear behavior can be observed for the pitch moment as the angle of attack is increased (in module) and this behavior can be explained considering the longitudinal vortices near the upper surface, for positive angle of attack, and near the lower one, for negative values of α. It must be remembered that the vortex strength is increased along its longitudinal axis, due the continuous vorticity generation along the model edge, where the vortex is originated. A consequence of the above explanation is a continuously pressure decrement along the model longitudinal axis, over the upper or lower surface, depending the angle of attack. For positive angle of attacks, such pressure variation is correlated to an upward force distribution, which continuously growth along the model axis and produce a negative pitch moment, which reduces the magnitude of the moment generated at the nose region, resulting a slight decrement in the moment derivative with respect to the angle of attack. The opposite behavior is observed for the negative angle of attacks.

The Cl x Cm curve is very important to the experimental determination of the aerodynamic center of any aerodynamic body. The results obtained to both fuselage models are shown in the Fig. 10 and, again, an erratic behavior is observed. Here, such behavior was amplified because lift, as well as, pitch moment are obtained with the same load cells and, them, the uncertainty of both measurements became more evident. Normally, the aerodynamic center is determined by using the angular coefficient of the linear region of the Cm x Cl curve. In the present case, due to the erratic behavior, the uncertainty associated to this parameter is large, but an approximate value can be determined. It is interesting to note that although Cl and Cm are different for both models for the same angle of attack, a coincidence is observed for the Cm x Cl curve. The longitudinal vortices strength do not have great influence on the aerodynamic center position, whose values are reported in the table 1. The X axis has origin at the fuselage nose and the model height (h) was used to define non-dimensional parameters presented at table 1.

Table 1: Non-dimensional aerodynamic center position and its uncertainty

Fuselage Model	Xac / h	δ_{Xac} / h
Sharp corner	0,8	0,2
Rounded corner	0,8	0,4

5. FINAL REMARKS

The main objective of the present paper is to report some aerodynamic data about the fuselage used at ITA´s Unmanned Aircraft Vehicle (UAV), which will be used to examine electric transmission lines, in order to improve the aircraft design methodology. This objective was reached by using a wind tunnel and two fuselage models, which have rectangular cross section and: (i) sharp corners and (b) rounded ones.

The flow field around the fuselage model was visualized by using wool tufts and longitudinal vortices, formed along the longitudinal model edges, are responsible by the non-linear behavior observed for the lift, drag and pitch moment results.

The sharp edge model generates more lift, drag and pitch moment for the same angle of attack when compared with the rounded edge model. Considering angle of attack equal to zero, the rounded edge model has 30% less drag coefficient than the other model and this is an important result of such research. The comparison between a semi-empirical method and experiments has shown over estimation of drag coefficient for α equal to zero degrees (approximately 40%)

One of the objectives of the flow visualization is the flow behavior over the lower surface of the trailing cone, which could separate due to an abrupt inclination variation that occurs at the interface between the constant cross section part and the trailing cone. For every angle of attack (ranging from -20 to +20 degrees) the flow observed was attached to the surface and them, wake drag is avoided. On the other hand, induced drag is observed due to longitudinal vortices generated at the edge formed by the intersection of the trailing cone lower wall and its lateral ones.

The semi-empirical method, normally used in the conceptual design phase, was applied to the fuselage model and its results were compared with the ones obtained experimentally in the present paper. The drag coefficient for angle

of attack equal to zero was greater than the ones obtained experimentally, with a difference of 40% approximately. The induced drag is under estimated when compared with the semi-empirical method, because the longitudinal vortices pattern, observed in the present paper, are not taken into account.

Finally, some erratic behavior was observed to the results for the lift and pitch moment coefficients and, as a consequence, the uncertainty of such parameters become relatively high. The problem is the load cells stiffness used to detect both parameters and, in future work, more flexible sensors will be used in order to get more reliable results.

6. ACKNOWLEDGEMENTS

To the Financiadora de Estudos e Projetos (FINEP), for supporting part of the resources used to the Unmanned Aircraft Vehicle development (protocolo 243/2004) and to the Centro de Estudos de Sistemas Avançados do Recife (CESAR), to the partnership in this project. To the staff of the Prof. K.L. Feng Aeronautical Engineering Laboratory: Carlos Guedes Neto, Luis Zambrano Lara, Vitor Valentim Betti and Mario Correia.

7. REFERENCES

Bearman, P.W. (1965): Investigation of the flow behind a two-dimensional model with a blunt trailing edge and fitted with splitter plates. *J. Fluid Mech*., Vol. 28, pp. 241-255.

Girardi, R.M. e Rizzi, P., (2005a), "Análise do tipo da aeronave mais adaptada para a inspeção de linhas de transmissão", Relatório de Trabalho, CESAR/ITA, 27 de junho.

Girardi, R.M. e Rizzi, P., (2005b), "Seleção da alternativa mais promissora para prova de conceito, através da construção e testes em vôo", Relatório de Trabalho, CESAR/ITA, 27 de junho.

Girardi, R.M. e Rizzi, P., (2006), "Desenvolvimento de Metodologia para Projeto Conceitual de um Veículo Aéreo Não Tripulado (VANT), Usado para Inspeção de Linhas de Transmissão de Energia Elétrica", Anais do Congresso Nacional de Engenharia Mecânica (CONEM), Recife, Pe.

Girardi, R.M. e Rizzi, P., (2006), "Projeto Conceitual de um Veículo Aéreo Não tripulado, Usado para Inspeção de Linhas de Transmissão de Energia Elétrica". Anais do 11º Encontro Nacional de Ciências e Engenharia Térmicas (ENCIT 2006), Curitiba, Dez. 5-8.

Kline, S.J. and McClintock, F. A. (1953): Describing uncertainties in single-sample experiments. *Mechanical Eng*., pp. 3-8.

Kubo,Y. et all.(1989): Effects of end plates and blockage of structural members on drag forces. *J. Wind Eng. Ind. Aerodynamics*, vol.32, pp.329-342.

Rae, W.H. and Pope (1984), A *Low speed wind tunnel testing*. Second edition, John Wiley & Sons, USA.

Raymer, D.P., (1999), "Aircraft design: a conceptual approach", AIAA Education Series, AIAA, Washington DC.

Roskam, J., (2000-2003), "Airplane design", parts I-VIII, Dar Corporation, Lawrence, Kansas, USA.

8. RESPONSIBILITY NOTICE

The authors are the only responsible for the printed material included in this paper.